Available online at www.sciencedirect.com
SCIENCE DIRECT
Polymer 46 (2005) 523–530
polymer
www.elsevier.com/locate/polymer

Influence of platelet aspect ratio and orientation on the storage and loss moduli of HDPE-mica composites

Albrecht Kuelpmann, Maged A. Osman, Lars Kocher, Ulrich W. Suter*

Department of Materials, ETH Zurich, CH-8093 Zurich, Switzerland

Received 24 June 2004; received in revised form 23 September 2004; accepted 23 September 2004
Available online 2 November 2004

Abstract

Composites of HDPE and glass or mica particles with different aspect ratios and surface modifications were prepared. The aspect ratio of the mica platelets was evaluated by image analysis of SEM micrographs. Test specimens, in which the platelet faces are oriented either parallel or perpendicular to the specimen flat surface, were prepared and the orientation of the particles was assessed by X-ray diffraction. Oscillatory rheological measurements in the linear viscoelastic regime were carried out. The in-plane and out-of-plane shear behavior was measured and the Halpin–Tsai structural parameter ζ calculated. For in-plane shear, ζ slightly decreased with increasing aspect ratio, whereas for out-of-plane shear, ζ strongly increased. Surface treatment of the mica particles had practically no influence on the results in the investigated loading range (volume fraction $\leq 7\%$).

Keywords: Aspect ratio; Modulus; Orientation

1. Introduction

The reinforcing potential of plate-like particles in polymeric materials has been recognized a long time ago and their micro-composites have been synthesized and investigated [1–4]. High-aspect-ratio muscovite and phlogopite were prepared and used at high loading to enhance the flexural properties of polymers. In the last decade, extensive research on nanocomposites has been carried out, in which the filler particles are plate-like with dimensions in the nanometer range [5]. This research focused on the synthesis of the composites and on relating their properties to the microstructure. However, some aspects are easier to tackle in micro-composites, which do not suffer from the problem of mixed morphology.

The portfolio of relevant properties of polymers filled with rigid particles is large. Concentrating on the rheological properties, one has to take into account that the polymer itself is a complex fluid; particles adding to the complexity due to their hydrodynamic influence. Particles may also interact with each other, or bind the polymer more or less strongly, and they may alter the properties of the polymer matrix itself through so-called confinement effects [6]. Multiscale-models have been developed to account for such effects [7,8]. Whereas many properties can be qualitatively understood in terms of these models, it is difficult to quantify the individual effects.

Understanding the hydrodynamic influence of particles is the basis for describing the behavior of filled polymers. At the simplest level, the parameter that characterizes the hydrodynamic influence of single particles in viscous flow is the Einstein coefficient or intrinsic viscosity [9]. Intrinsic viscosities for mica filled polymers were determined by Utracki et al. [10]. Plastic disks dispersed in Newtonian liquids were investigated by Lingard and Whitmore [11] and data for hardened red blood cells in aqueous medium were obtained by Chien et al. [12]. Based on these results, Utracki et al. [10] proposed a correlation between the aspect ratio and the intrinsic viscosity. Although it was recognized that the orientation of the particles with respect to the flow direction plays an important role, it was not included in the evaluation of the results.

For a constitutive description, it is usually surmised that a

* Corresponding author. Tel.: +41 44 632 2039; fax: +41 44 632 1592.
E-mail address: uwsuter@eth.ch (U.W. Suter).

0032-3861/$ - see front matter © 2004 Elsevier Ltd. All rights reserved.
doi:10.1016/j.polymer.2004.09.056

composite with oriented disk-shaped particles is transversely isotropic. Therefore, the shear behavior is characterized by in-plane and out-of-plane behavior. For instance, if particles are preferentially oriented in-plane to the shear deformation, the effects of misalignment can be understood if the out-of-plane shear behavior is known.

In this study, HDPE-mica composites with the particles oriented parallel or perpendicular to the flat sample surface were prepared and their rheological properties investigated. The degree of alignment was assessed by wide angle X-ray diffraction (WAX). The aspect ratio (diameter/thickness) of the particles in the composite was evaluated by image analysis of SEM micrographs. The two shear moduli of the transversely isotropic compounds were measured in the molten state and compared to the widely used Halpin-Tsai model [13].

2. Background

2.1. Micromechanical models for elasticity

The elastic properties of a transversely isotropic sample, as in a composite of a polymer and randomly distributed, unidirectionally oriented disks, can be described by five independent constants. With engineering notation, the longitudinal and transverse Young's modulus (E_{11} and E_{22}), the in-plane and out-of-plane shear moduli (G_{23} and G_{12}), and the longitudinal Poisson's ratio ν_{12} can be used [13,14]. A simple and widely used empirical model to calculate the relative modulus (composite modulus/matrix modulus) of a composite is the Halpin-Tsai model [13]. Following the notation by Halpin, the relative modulus can be written as

$$\frac{M}{M_{\mathrm{m}}} = \frac{1 + \varsigma\eta\phi}{1 - \eta\phi}, \quad \text{with } \eta = \frac{(M_{\mathrm{f}}/M_{\mathrm{m}}) - 1}{(M_{\mathrm{f}}/M_{\mathrm{m}}) + \varsigma} \tag{1}$$

where M stands for a modulus, the indices m and f denote properties of the matrix and the filler, respectively, ϕ is the volume concentration of the filler and ζ is a model parameter ($0 \leq \zeta < \infty$). For the cases of interest in this study, the polymer's moduli are orders of magnitude lower than those of the filler and η becomes 1.

The strong analogy between the mechanical behavior of composites and the flow of dispersions has often been noted [15]. Along this line Nielsen [16] showed that for very small filler concentration, ζ can be related to the value of the Einstein coefficient k by

$$\zeta = k - 1 \tag{2}$$

The empirical parameter ζ is correlated with the geometry of the reinforcement and can be evaluated by fitting experimental data to Eq. (1). This allows to conveniently employ Eq. (1) for particles with different aspect ratios. The Halpin–Tsai equation has been fitted to numerical data for such systems and a widely used program to calculate elastic moduli of reinforced materials (LITAC) uses that relation to evaluate ζ as a function of aspect ratio α [17]. According to Halpin [18], for out-of-plane shear:

$$\zeta = \alpha^{1.732} \tag{3}$$

For in-plane shear the same relation holds with $1/\alpha$ instead of α. It has to be noted that Eq. (3) is the result of a fitting exercise and for spheres, where α equals 1, it does not agree with the well established Kerner [19] result, $\zeta = 1.5$.

2.2. Application to viscoelastic materials

The Halpin–Tsai equation as well as all other models for elastic behavior assumes boundaries, where the deformation rate at the filler surface is zero and the stress is in equilibrium. However, in viscous materials slip may occur. For slip conditions, stress is not completely transferred at interfaces and the reinforcement decreases. No quantitative theory has been developed yet to account for such effects on the modulus but we assume that concepts developed for the viscosity of filled polymers can be at least qualitatively applied here [20].

The same relations as for elastic media should hold for viscoelastic media if we consider the matrix as a polymer network, visualized as a generalized Maxwell-body, i.e. if we only consider the linear viscoelastic regime [21]. The elastic and viscous response as a function of applied shear frequency ω is then given by a summation of Maxwell elements as the storage modulus $G'(\omega)$ and the loss modulus $G''(\omega)$, respectively, [22].

$$G'(\omega) = \sum_{i=1}^{N} \frac{g_i \lambda_i^2 \omega^2}{1 + \lambda_i^2 \omega^2} \quad \text{and} \quad \mathrm{G''}(\omega) = \sum_{\mathrm{i}=1}^{\mathrm{N}} \frac{\mathrm{g_i}\lambda_{\mathrm{i}}\omega}{1 + \lambda_{\mathrm{i}}^2\omega^2} \tag{4}$$

where i is the index of the relaxation mode, g_i the modulus of a particular relaxation mode and λ the associated relaxation time. In Eq. (4) g_{i} is independent of frequency and serves as a link between frequency independent elasticity and frequency dependent viscoelasticity. Eq. (1) can be applied to express each g_{i} for a filled polymer, where M and M_{m} are replaced by g_{i} for the filled polymer and g_{mi} for the matrix. In a more general context, this is known as the elastic-viscoelastic correspondence principle [14]. If the rigid inclusion does not contribute to the viscoelastic response of the sample in another way, e.g. by additional relaxations, it increases each relaxation modulus (for a given filler loading) by the same factor that can be factored out of the summation [7]. Consequently, the relative modulus is independent of frequency. Therefore, it can be expected that as long as changes in the relative modulus are frequency independent, they are of hydrodynamic nature. The relations for the storage modulus should equally hold for the loss modulus, since they are both linear in g_{i} and the same factorization can be carried out. This implies that

applying micromechanical models for the elasticity of a composite also reveals information on the viscous response.

3. Experimental section

3.1. Materials

The HDPE used in this study is Hostalen GF 9055F obtained from Basell–Polyolefins (Wesseling, Germany). It has a density of 0.954 g/cm^3 at room temperature. Wet ground muscovite mica R120 and SX400 were obtained from Microfine Minerals (Derby, UK), while S11 was prepared by milling a concentrated slurry of Samica 11 mica paper, that was supplied by von Roll Isola (Breitenbach, Switzerland). Glass microspheres with an average diameter of 22 μm (Spheriglass 3000) were delivered by Potters–Ballotini (Düsseldorf, Germany). A list of the different fillers used is given in Table 1.

3.2. Powder preparation

For measuring the size distribution of plate-like particles by image analysis, it is preferable to have a relatively narrow size distribution. Therefore, the ground mica particles were subjected to a sedimentation process. 100 g of mineral was dispersed in 10 L of deionized water in a 10 L beaker and left to settle for four hours, after which the supernatant liquid was removed. The remaining mineral was re-suspended in 10 L water and the sedimentation procedure repeated with consecutive settling times of 3, 2, and 1 h. Only the largest particles were collected, dried, and sieved with a 60 μm sieve. A part of the R120 particles was surface modified by exchanging their inorganic cations with organic ammonium ions according to the method described by Osman et al. [23]. These particles are denoted R120·2C18 for dimethyldioctadecylammonium-modified particles and R120·BzC16 for benzyldimethylhexadecylammonium-modified particles.

3.3. Sample preparation

The polymer and filler were compounded in a Brabender internal mixer 'Plasti-Corder W 50 EH' (Brabender, Duisburg, Germany) equipped with a 30 cm^3 bowl and counter-rotating blades. The polymer pellets were molten at 150 °C and the filler was slowly added within 5 min. The mixture was then kneaded for 10 min at 60 rpm. Care was taken to fill the mixer cell completely with material to ensure optimal mixing and avoid incorporation of air into the composite.

Table 1
Fillers and their surface modification

Filler type	Surface modification
S11	No
R120	No
R120·2C18	Dimethyldioctadecylammonium
R120·BzC16	Benzyldimethylhexadecylammonium
SX400	No
Spheriglass	No

Test specimens with a strong orientation of the flat surface of the platelets (face) were prepared. For specimens in which the faces of the platelets are oriented parallel to the sample flat surface, the compound was compression molded at 170 °C in an aluminum frame of dimensions 130×130×1.5 mm. After cooling, the sheet was cut into four pieces of equal size and compression molded again in the same frame. This process was repeated four times. By this procedure the composites experienced large strains that led to a high degree of orientation of the particles and homogeneous orientation throughout the sample. For rheological testing, circular disks of 20 mm diameter were stamped out of the composite sheets. For specimens with the particles' faces oriented perpendicular to the sample flat surface, rectangular sheets of dimensions 20×20×1.5 mm were cut. The sheets were stapled in a frame of dimensions 25×25×30 mm and molded to cubes at 170 °C under argon. Cylinders of 20 mm diameter were mill cut out of the cubes and sliced to circular disks of 1.5 mm thickness. The above described procedure is sketched in Fig. 1. The neat polymer was subjected to the same process to check for possible thermal or mechanical degradation. However, no change in viscosity was observed compared to a virgin polymer sample.

3.4. Scanning electron microscopy (SEM) and image analysis

To study the morphology of the composites, the face of a

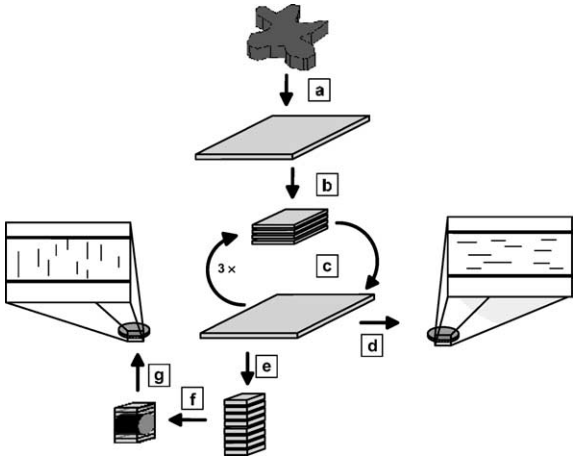

Fig. 1. Sample preparation, (a) compression molding at 170 °C, (b) cut to four equally sized plates, (c) compression molding (b and c are repeated three times), (d) cutting circular disks, in which the platelets are oriented parallel to the flat sample surface, (e) cut to small equally sized plates, (f) molding to cube, (g) mill-cutting cylinder and disks, in which the platelets are oriented perpendicular to the flat sample surface.

sample cut perpendicular to the flat sample surface was planed with a diamond knife of a microtome (Reichert Jung Ultracut E). The sample face was etched with cold oxygen plasma for 3 min to enhance the contrast. The sample surface was sputter coated with 3 nm of Pt and observed in a LEO 1530 Gemini 'in-lens' field emission scanning electron microscope (FESEM) at 5 kV accelerating voltage. Images were taken at magnifications ranging from 2500 to 5000 and analyzed with the software analySIS© (Soft Imaging System GmbH, Munster, Germany) with manual detection. Each sample was characterized by the evaluation of at least 1000 particles.

3.5. X-ray diffraction

To characterize the orientation of the filler particles with respect to the sample flat surface, rocking curves were measured. The experiments were performed on a Scintag PAD X powder diffractometer using Cu K_α radiation ($\lambda = 1.5418$ Å). For specimens with the platelet faces oriented parallel to the sample surface, square sheets (from step c in Fig. 1) were subjected to the measurement directly. For specimens with the platelets oriented perpendicular to the flat sample surface, a 1.5 mm slice of the cube (from step f in Fig. 1) was cut parallel to the plane of the sheets from which the cube is made. The (004) reflection of mica is well suited for characterizing the degree of orientation of the filler, because the (004) plane lies parallel to the platelet surface and its 2θ value allows a relatively wide tilt angle to be investigated. In a standard $\theta-2\theta$ scan, the exact 2θ position of the (004) reflection of mica was determined. Rocking curves were measured with the detector set at the 2θ position by tilting the rotating sample in steps of 0.1° over a range of $2-16°$ 2θ and counting for 2 s at each step. From the linear absorption coefficient of polyethylene and mica the penetration depth of the X-ray beam was calculated to be in the order of 0.1 mm for the range of tilt angles investigated [24].

3.6. Rheological testing

For rheological measurements, a Paar Physica rheometer MR 300 with parallel plate ($d = 50$ mm) geometry was used. Small strain oscillatory shear experiments were performed at 170 °C under nitrogen atmosphere. Data were collected at strain amplitude of 1%. At this amplitude, all composites showed linear viscoelastic behavior as determined by amplitude sweep experiments. The observed frequency range was from 628 rad/s, decreasing logarithmically, to 0.068 rad/s. From the rheological response, $G'(\omega)$ and $G''(\omega)$ were obtained. For specimens, in which the particles were oriented parallel to the sample surface (sample d in Fig. 1), shearing in a torsional rheometer yielded in-plane moduli, whereas for those, in which the particles were oriented perpendicular to the sample surface (sample g in Fig. 1), it yielded out-of-plane moduli.

4. Results and discussion

4.1. Image analysis

The dimensions of the particles in the composite were determined by image analysis of SEM micrographs of samples with ca. 7 vol% loading. From this analysis, reliable data on $p(D)$, the distribution of particle diameters D, and $p(\alpha)$, the distribution of aspect ratios were obtained. A computer model of a sample and the corresponding surface are sketched in Fig. 2a and b. A SEM micrograph of a sample surface (R120) is shown in Fig. 2c. For data analysis, it is assumed that the particles are perfectly oriented and disk-shaped. Cutting a circular disk perpendicularly to its flat surface gives a cut edge of length l. If the cut runs at a distance x from the centre, l is given by

$$l = \sqrt{D^2 - 4x^2} \tag{5}$$

To find the probability density of l for particles of the same diameter D, we follow Russ [25] and consider that the platelets are positioned at random in the sample and therefore, the cut would occur at any $0 \le x \le D/2$ with the same probability, i.e. $p_D(x)$ is a constant that takes the value $-2/D$ after normalization. To obtain $p_D(l)$, $p_D(x)$ has to be expressed as a function of l.

$$\int_0^D p_D(l)\mathrm{d}l = \int_{D/2}^0 p_D(x(l))\frac{\mathrm{d}x}{\mathrm{d}l}\mathrm{d}l = 1 \tag{6}$$

$\mathrm{d}x/\mathrm{d}l$ can be calculated from Eq. (5) and the probability to find a length within the interval l_1 and l_2 with l_1 and $l_2 \le D$ yields

$$\begin{aligned}\int_{l_1}^{l_2} p_D(l)\mathrm{d}l &= \int_{l_1}^{l_2} \frac{l}{D\sqrt{D^2 - l^2}}\mathrm{d}l \\ &= \frac{1}{D}\left(\sqrt{D^2 - l_1^2} - \sqrt{D^2 - l_2^2}\right)\end{aligned} \tag{7}$$

In practice, not only one diameter D is present, but D is size distributed. The distribution of lengths for all diameters, $p(l)$, can then be expressed as a product of both distribution functions $p_D(l)$, Eq. (7), and $p(D)$

$$p(l) = \int_D p_D(l)p(D)\mathrm{d}D \tag{8}$$

Dividing the lengths l and diameters D into discrete steps (Δl and ΔD) yields approximately

$$p(l)\Delta l \propto \sum_j p_D(l)\Delta l p(D)\Delta D_j \tag{9}$$

$p(l)\,\Delta l$ is given by the measured data. The best fit of $p(D)$ to Eq. (9) represents the distribution density of diameters for the investigated surfaces [25].

For the mechanical properties of a composite, not only the volume of a given particle is of importance but also its geometry that is characterized by the aspect ratio (ratio of

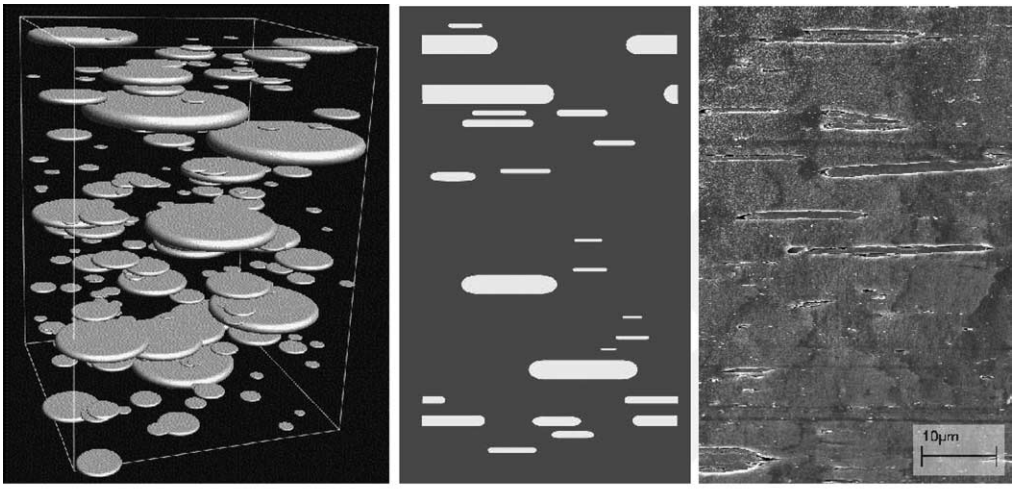

Fig. 2. (a) computer-generated model with disk-shaped inclusions. (b) virtual cut through a computer generated structure (aspect ratio 10). (c) SEM micrograph of R120 composite (from step *d* in Fig. 1).

diameter D to thickness t). The mean thickness of particles with cut length l is given by the measured data

$$\langle t(l)\rangle = \frac{\sum_j t_j(l)}{\sum_j j} \tag{10}$$

The mean thickness can also be given by the mean of the thicknesses t weighted with the probability to have a particle of diameter D and cut it at length l. For discrete steps in D and l, this yields

$$\langle t(l)\rangle = \frac{\sum_j t(D)p_D(l)\Delta l p(D)\Delta D_j}{\sum_j p_D(l)\Delta l p(D)\Delta D_j} \tag{11}$$

The function $t(D)$ is fitted so that Eq. (11) becomes the best representation of the measured data. This yields an aspect ratio for each diameter class, ΔD_j, with the probability $p(D_j)$. The fitting results represent the number-weighted distribution of diameters D and corresponding thickness $t(D)$ for the particles on the cutting surface. These surface distributions are converted to the corresponding distribution per volume element by

$$p_{\mathrm{Vol}}(D) \propto \frac{p_{\mathrm{Surf}}(D)}{D} \tag{12}$$

$p_{\mathrm{Vol}}(D)$ and $p_{\mathrm{Surf}}(D)$ are the number-weighted distributions per volume element and per surface element, respectively. The distributions must be weighted with the reciprocal diameter since larger particles are more likely to appear on the cutting surface than smaller particles, proportional to D. The number-weighted distribution per volume element can be converted to differently weighted distributions.

As an example, the volume-weighted distributions of diameter and aspect ratio are given for S11 in Fig. 3. The figure shows the diameters with its associated aspect ratio α in the base plane. The height of the stems represents the distribution density. The volume weighted-aspect ratio distribution is projected onto the left back plane, the volume weighted diameter distribution onto the right back plane. The average results for the mica particles used in this study are listed in Table 2. Comparing the volume-weighted averages: SX400 is smallest in diameter and aspect ratio, R120 and S11 have the same aspect ratio but R120 is considerably larger in diameter. Taking the ratio of the volume- and number-weighted quantities as a measure for the distribution width, SX400 has the narrowest distribution of diameter and aspect ratio. R120 and S11 have the same distribution width for the aspect ratio, but R120 has a broader diameter distribution.

4.2. X-ray diffraction

The rocking curves are direct measures of the orientation of the (004) reflection planes, which run parallel to the mica

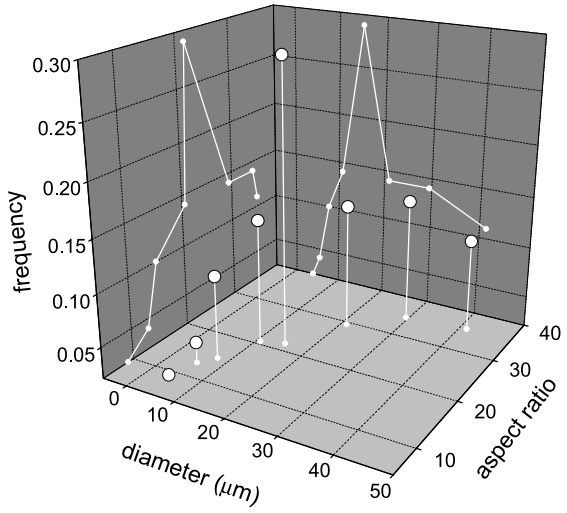

Fig. 3. Distribution of volume-weighted diameter and aspect ratio for S11 composite from image analysis. In the base plane, the relation of diameter to aspect ratio can be seen.

Table 2
Comparison of the mean diameters D, aspect ratio α, and orientation distribution of the mica grades used

Filler	D_N (μm)	D_V (μm)	α_N	α_V	$\beta_{\parallel}$ (°)	$\beta_{\perp}$ (°)
S11	6.2	19	12	24	4.5	6.7
R120	6.2	29	12	24	4.3	5.9
SX400	8.8	13	5.8	9.1	4.7	5.9

N, denotes number-weighted average and V, volume-weighted average. Orientation distributions are given as full-width-at-half-maximum values (β) with respect to the intended orientation.

surface. In all cases, the highest intensity is found for the orientation parallel to the surface of the sample. To assess the degree of particle orientation, the full-width-at-half-maximum, β, was determined for each of the rocking curves using a pseudo-Voigt (a linear combination of a Lorentzian and Gaussian function) peak fit (Fig. 4) [26]. Approximately 60% of the particles lie within the range given by β, and ca. 80% within 2β. The values obtained for specimens with filler particles oriented parallel to the main surface ($\beta_{\parallel}$) and for the samples cut from the cube after compression molding ($\beta_{\perp}$) are summarized in Table 2. For the first set of samples ca. 80% of the particles lie within 5° of the intended orientation. As might be expected, the orientation after molding in cubes has deteriorated somewhat, presumably as a result of imperfect alignment of the stacked sheets (step *e* in Fig. 1). In the worst case (S11), ca. 80% of the particles still lie within 7° of the intended orientation.

Since particles oriented perpendicular to the surface may be distorted by bringing the sample into contact with the rheometer tool, a 3D texture analysis was performed on two samples, one taken from the surface and one from the middle of the R120 composite after rheological measurement (data not shown). These data were collected in transmission mode on the Swiss–Norwegian Beamline at the European Synchrotron Radiation Facility in Grenoble. The results indicate that the orientation distribution at the surface of the sample, where it comes in contact with the rheometer tool is wider than in the middle of the sample, but it is not possible to quantify this effect.

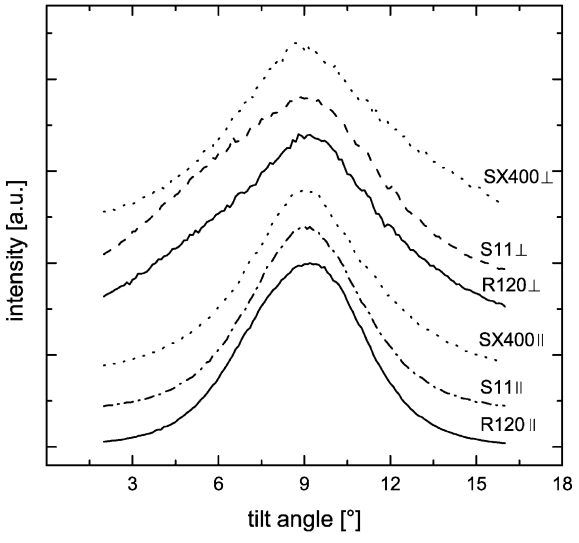

Fig. 4. Rocking curves for specimens with mica particles oriented parallel and perpendicular to the specimen flat surface.

4.3. Rheology

The relative storage and loss moduli of the composites, in which the particles are oriented perpendicular to the sample flat surface, are plotted in Fig. 5 as a function of shear frequency for filler loading up to ca. 11 vol%. In the low frequency range, the reduced moduli show frequency dependence even at the lowest filler loading, while at high frequencies, dependence can only be seen for filler loading >7 vol%. In the linear viscoelastic regime, hydrodynamic forces are dominant if the modulus-frequency relationship is only vertically shifted, i.e. the relative modulus is frequency independent. This study concentrates on the hydrodynamic contribution of the filler and the data interpretation will be limited to the highest shear frequency of 86 rad/s for composites with filler loading ≤ 7 vol%. For illustration, these data are marked in Fig. 5.

Linearization of the measured data according to Eq. (1) ($\eta \approx 1$, since $M_f/M_m \gg 1$) with respect to the filler volume fraction ϕ, yields the parameter ζ as the slope. Data for the storage moduli of S11 composites are plotted in Fig. 6. Squares represent the systems with particles aligned parallel to the sample's flat surface; circles represent systems with

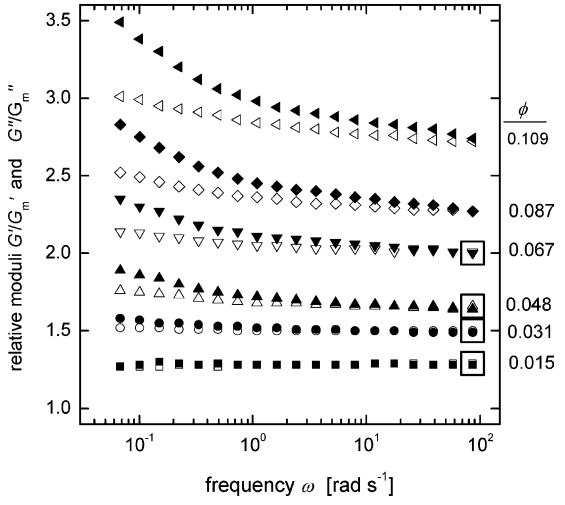

Fig. 5. Reduced storage and loss moduli (open and closed symbols, respectively) of perpendicularly oriented S11 composites with different loading as a function of shear frequency. Boxed data points are discussed further in this study.

particles aligned perpendicular to the same surface. The error bars show the standard deviation for the average of three measurements. Results for the loss moduli are identical to those of the storage moduli for all samples, as expected for a generalized Maxwell fluid. A straight line fit through the origin for all samples holds very well. The slope ζ for the loss and storage moduli of all systems (parallel and perpendicular oriented particles) is given in Table 3. Fig. 6 and Table 3 show that as long as the dependence of storage modulus on aspect ratio is small, as for in-plane shear, the average error in the slope is ca. 30%, whereas for particles with perpendicular orientation, the average error in ζ is only 10%.

The relation between the parameter ζ and the volume-weighted aspect ratio α is shown in Fig. 7 for the unmodified fillers. A strong dependence of ζ on aspect ratio in the case of perpendicularly oriented particles and a weak dependence for parallel oriented particles can be seen. For the spherical glass particles, the results are close to those predicted from theory ($\zeta = 1.5$ at $\alpha = 1$) [19]. The slight deviation is probably due to the limited number of measurements. In contrast, the results for disk-shaped particles do not agree with predictions from Eq. (3). For out-of-plane shear, the experimental data show a linear trend of ζ with α in the examined concentration range, while for in-plane shear the results and predictions exhibit a weak negative dependence of ζ on aspect ratio. The results for G' and G'' are quite similar and the data suggest the following relations for both, ζ of G' and ζ of G'':

$$\zeta_{\parallel}(\alpha) = 1.99 - 0.03\alpha \quad \text{and} \quad \zeta_{\perp}(\alpha) = 1.54 + 0.42\alpha \qquad (13)$$

where α is the volume-weighted average aspect ratio.

The influence of surface treatment of the filler on ζ was also studied. In general, a surface modification that does not react with the polymer decreases the matrix–filler interaction [27]. This would lead to a decrease in ζ. The corresponding data are plotted in Fig. 8 for R120, R120·2C18 and R120·BzC16. Compared to the unmodified filler, the surface treatment with dimethyldioctadecylammonium and bezyldimethylhexadecylammonium, respectively, gives the same results within the experimental error. The data suggest that the specific polymer/particle interactions or slip/no slip conditions do not exhibit a noticeable effect at this filler loading.

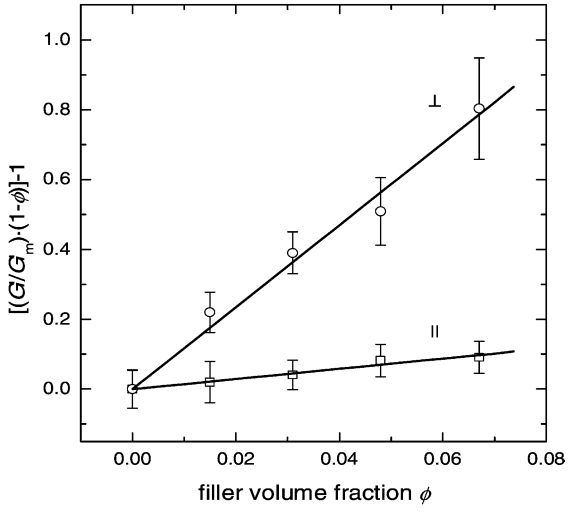

Fig. 6. Storage moduli of S11 composites as a function of filler volume fraction. Squares represent particles oriented parallel to the sample flat surface, while cirlces stand for particles oriented perpendicular to the surface. The slope of the linear fit represents the parameter ζ in Eq. (1) (since $\eta \approx 1$). Error bars indicate the standard deviation in the measurements.

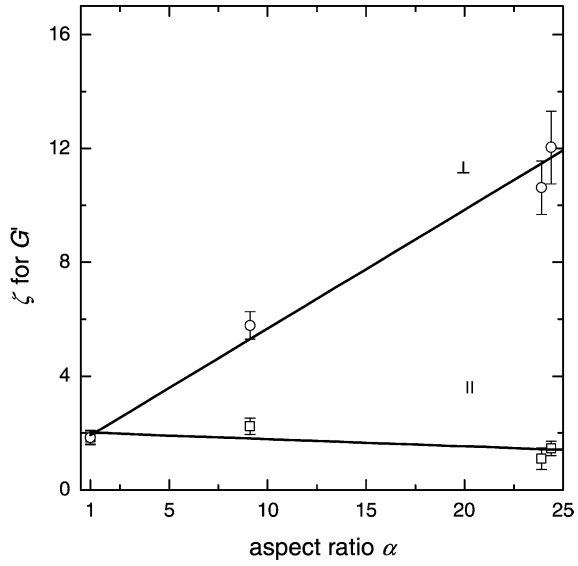

Fig. 7. Parameter ζ as a function of the volume-weighted average aspect ratio for the storage modulus. Squares represent particles oriented parallel to the sample flat surface, while circles stand for particles oriented perpendicular to the sample surface.

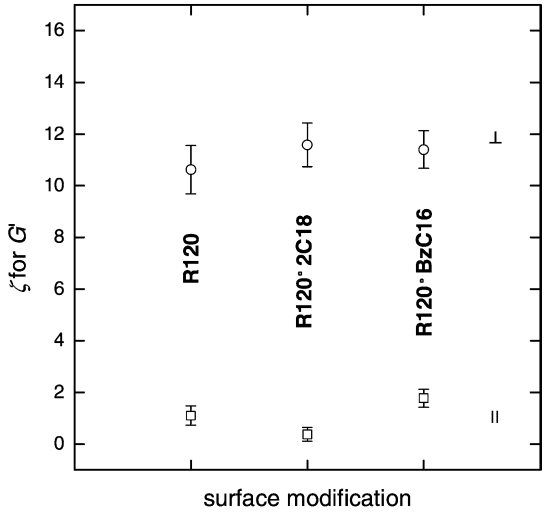

Fig. 8. Parameter ζ as a function of surface treatment for the storage modulus. Squares represent particles oriented parallel to the sample flat surface, while circles stand for particles oriented perpendicular to the sample surface.

Table 3
Comparison of parameter ζ for G_{23}', G_{23}'', G_{12}', and G_{12}''

Filler	ζ for G_{23}'	ζ for G_{23}''	ζ for G_{12}'	ζ for G_{12}''
S11	1.5(±0.3)	1.3(±0.3)	12.0(±1.3)	12.4(±1.4)
R120	1.1(±0.4)	1.1(±0.4)	10.6(±0.9)	11.0(±1.1)
R120·2C18	0.4(±0.3)	0.3(±0.3)	11.6(±0.8)	11.4(±0.7)
R120·BzC16	1.8(±0.4)	1.6(±0.4)	11.4(±0.7)	11.7(±0.7)
SX400	2.2(±0.3)	2.0(±0.3)	5.8(±0.5)	6.1(±0.6)
Spheriglass	1.8(±0.3)	1.9(±0.3)	1.8(±0.2)	1.8(±0.2)

The associated probable error is given by the uncertainty of the slope in the linear regression.

5. Conclusion

The storage and loss moduli of plate-like particle-filled HDPE strongly depend on the orientation of the platelets with respect to the shear direction. Hence, the description of the orientation is essential for the characterization of such composites. Both moduli show the same dependence on filler loading, aspect ratio and orientation. Out-of plane shear moduli strongly increase with increasing aspect ratio, whereas in-plane moduli slightly decrease. The concentration dependence of the moduli is well represented by the Halpin–Tsai equation with ζ as an adjustable parameter. ζ serves as a parameter that characterizes the potential of plate-like particles with a certain orientation to influence the elastic and viscous properties of the composites. It can be correlated with the aspect ratio by the following equations:

$$\zeta_{\parallel}(\alpha) = 1.99 - 0.03\alpha \quad \text{and} \quad \zeta_{\perp}(\alpha) = 1.54 + 0.42\alpha$$

Acknowledgements

We would like to thank M. Müller for his expertise in electron microscopy and H.R. Lusti for the computer simulation. Experimental assistance from the staff of the Swiss–Norwegian Beamlines at the European Synchrotron Radiation Facility in Grenoble is gratefully acknowledged. We also acknowledge financial support from the Swiss National Science Foundation (SNF).

References

[1] Lusis J. The Importance of flake aspect ratio in mica reinforced plastics MSc: University of Toronto; 1971.
[2] Lusis J, Woodhams RT, Xanthos M. Polym Eng Sci 1973;13(2):139.
[3] Maine FW, Sheperd PD. Composites 1974;5:193–200.
[4] Kauffman SH, Leindern J, Woodhams RT, Xanthos M. Powder Technol 1974;9:125–33.
[5] Kojima Y, Usuki A, Kawasumi M, Okada A, Fukushima Y, Kurauchi T, Kamigaito O. J Mater Res 1993;8(5):1185–9.
[6] Nelson RD. Dispersing Powders in Liquids, vol. 7. Amsterdam: Elsevier; 1988.
[7] Leonov AI. J Rheol 1990;34(7):1039.
[8] Sheng N, Boyce MC, Parks DM, Rutledge GC, Abes JI, Cohen RE. Polymer 2004;45:487–506.
[9] Larson RG. The Rheology of Complex Fluids. New York: Oxford University Press; 1999.
[10] Utracki LA, Favis BD, Fisa B. Polym Compos 1984;5(4):277.
[11] Lingard PS, Whitemore RL. Chemeca 1970;70:11–24.
[12] Chien S, Usami S, Dellenback RJ, Gregersen MI. Science 1967; 157(3790):827–9.
[13] Halpin JC, Kardos JL. Polym Eng Sci 1976;16(5):344–52.
[14] Christensen RM. Mechanics of composite materials. Florida: Krieger Publishing Company; 1991.
[15] Russel WB, Sperry PR. Prog Org Coat 1994;23:305–24.
[16] Nielsen LE. J Appl Phys 1970;41(11):4626.
[17] Bay RS. Fiber orientation in injection molded composites: a comparison of theory and experiment. PhD. Urbana-Champaign; 1991.
[18] Halpin JC. Primer on composite materials analysis. Lancaster: Technomic; 1992.
[19] Kerner EH. Proc Phys Soc 1956;69:808–13.
[20] Inn YW, Wang SQ. Langmuir 1995;11:1589–94.
[21] Ferry JD. Viscoelastic properties of polymers. New York: Wiley; 1980.
[22] Morrison FA. Understanding rheology. New York: Oxford University; 2001.
[23] Osman MA, Ploetze M, Suter UW. J Mater Chem 2003;13:2359–66.
[24] Macgillavry CH, Rieck GD, Lonsdale K, editors. International Tables for X-Ray Crystallography. Physical and Chemical Tables, vol. 3. Birmingham: The Kynoch Press; 1962.
[25] Russ JC. Practical Stereology. New York: Plenum; 1986.
[26] Thompson P, Cox DE, Hastings JB. J Appl Cryst 1987;20:79.
[27] Pukanszky B, Fekete E. Adv Polym Sci 1999;139:109–53.